

# Journal of Materials Chemistry A

Accepted Manuscript



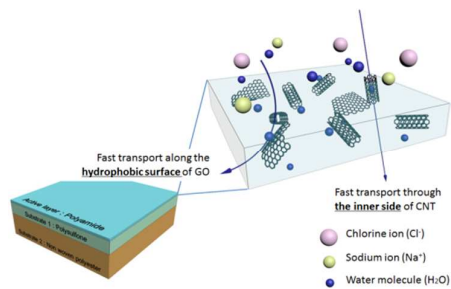
This is an *Accepted Manuscript*, which has been through the Royal Society of Chemistry peer review process and has been accepted for publication.

*Accepted Manuscripts* are published online shortly after acceptance, before technical editing, formatting and proof reading. Using this free service, authors can make their results available to the community, in citable form, before we publish the edited article. We will replace this *Accepted Manuscript* with the edited and formatted *Advance Article* as soon as it is available.

You can find more information about *Accepted Manuscripts* in the [Information for Authors](#).

Please note that technical editing may introduce minor changes to the text and/or graphics, which may alter content. The journal's standard [Terms & Conditions](#) and the [Ethical guidelines](#) still apply. In no event shall the Royal Society of Chemistry be held responsible for any errors or omissions in this *Accepted Manuscript* or any consequences arising from the use of any information it contains.

## Table of contents



Nanocomposite membrane containing CNT and GO exhibits much improved performances by the synergistic combinations of CNT and GO, which can increase the dispersity in polymeric matrix.

# High-Performance Reverse Osmosis Nanocomposite Membranes Containing the Mixture of Carbon Nanotubes and Graphene Oxides

Cite this: DOI: 10.1039/x0xx00000x

Received 00th January 2012,  
Accepted 00th January 2012

DOI: 10.1039/x0xx00000x

[www.rsc.org/](http://www.rsc.org/)

Hee Joong Kim, Min-Young Lim, Kyung Hwa Jung, Dong-Gyun Kim, and Jong-Chan Lee\*

Polyamide reverse osmosis membranes containing carbon nanotube with acidic groups (CNTa), graphene oxide (GO), and both of CNTa and GO (CNTa/GO) were prepared by the interfacial polymerization of the trimesoyl chloride solutions in hexane and the *m*-phenylenediamine aqueous solutions containing the carbon nanomaterials. All of the polyamide membranes containing the carbon nanomaterials showed much improved membrane performances such as water flux, chlorine resistance, long-term durability, and mechanical properties compared to the polyamide membrane without any of the carbon nanomaterials due to the advantageous properties of the CNT and GO as the filler materials. The largest improvement of membrane performances was observed from the polyamide membrane with CNTa/GO (the mixture of CNTa and GO). Since CNTa/GO can be more well-dispersed in the aqueous solution than the one component carbon nanomaterials such as CNTa and GO due to the surfactant effects of GO, and then the polyamide membrane with CNTa/GO can contain the largest amount of the carbon materials among the membranes and showed the largest membrane performances.

## 1 Introduction

Desalination, the production of fresh water from sea water or brackish water, has been known to be one of the most important and challenging issues in the environmental engineering and science fields because of the current water shortage problems.<sup>1-8</sup> The number of desalination plants using reverse osmosis (RO) membrane processes have increased over the past several years due to the advantages of membrane processes, such as low operating temperature, low energy consumption, and high production efficiency.<sup>5</sup> Polyamide membranes synthesized from interfacial polymerization have been the most widely used as RO membranes because of their high salt rejection combined with reasonably high water flux.<sup>8</sup> However, they have several disadvantages for desalination processes, such as low chlorine resistance and low antifouling properties, resulting in reduction of the membrane life and decrease of membrane performances such as water flux and salt rejection capabilities.<sup>8,9</sup> Therefore, there is a high requirement for the development of high-flux RO membrane systems with long term stability.<sup>10-12</sup>

Carbon nanotube (CNT) has been widely used as a filler material for the polymer nanocomposites to impart biocidal properties, thermal stability, and mechanical strength.<sup>13-18</sup> Furthermore, it was recently demonstrated by experimental and simulation results that polymer membranes containing CNTs can have very high water permeability because of the unique hydrophobic surface properties of the carbon nanomaterials.<sup>19-21</sup> Therefore, the polymeric films containing vertically aligned

CNTs and polymer nanocomposite membranes having well-dispersed CNTs have been investigated for possible application in water purification systems. Since it is difficult or even impossible to prepare the polymeric membranes with aligned CNTs having large enough effective membrane area, polymer nanocomposite membranes having well-dispersed CNTs has been investigated more widely for possible practical applications.<sup>11,22-26</sup> For example, polyamide RO membranes containing well-dispersed CNTs modified by strong acids or poly(dopamine) showed higher water flux than those without CNTs.<sup>11,23</sup> Modification of the CNTs was a prerequisite for the preparation of polyamide active layers containing well-dispersed CNTs without any aggregated clusters by the CNTs. When the CNTs are well-dispersed in the active layer, the increase of CNT contents causes an increase in the water flux without a decrease of the salt rejection if any. However, when the CNTs form aggregated clusters in the active layers, the polyamide membranes lose their salt rejection properties because of the large voids formed by the CNT clusters. Therefore, the best RO membrane performance showing very high water flux without losing the salt rejection property could be achieved when the largest amounts of CNTs are well-dispersed in the polyamide active layers.

Graphene oxide (GO) also has been widely studied as one of the important carbon nanofiller materials for polymer nanocomposites due to its extraordinary reinforcing efficiency of the electronic, thermal, and mechanical properties.<sup>15, 27-30</sup> In addition, graphene oxide (GO) can work as a surfactant to

increase the dispersion of CNTs in the polymer matrix, as the oxygen functional groups and the hydrophobic carbon structures in GO can increase compatibility with the polar polymers and the CNTs, respectively.<sup>30-34</sup> Therefore, various polymer nanocomposites containing both CNT and GO have been developed and studied regarding applications in batteries, sensors, and electronic device fabrication, as well as membranes.<sup>30-33, 35</sup> Recently, we also found that polyamide RO membranes containing both CNT and GO showed much better membrane performance than those containing only one of the two. In this manuscript, the preparation, physical properties, and membrane performances of polyamide membranes containing both of CNT and GO are described and compared with those of containing only CNT or GO, and those without the inclusion of any carbon nanomaterials.

## 2 Experimental section

### 2.1 Materials

Multi-walled carbon nanotubes (CNTs) were purchased from Nanocyl (Belgium). The average diameter and average length of CNT are 10 – 20 nm and 10 – 20  $\mu\text{m}$ , respectively. Graphites were received from BASF (Germany) for used as graphene oxide (GO) precursor. Polysulfone (PSf) membranes were supplied from Woong-jin chemicals (Republic of Korea) and used for a support membrane of the thin film composite membranes. The PSf membrane was composed of two layers, polysulfone and non-woven polyester layer. The commercial membrane for brackish water filtration was received from Hydranautics and its model name is LFC-1 (Low Fouling Composite). Sulfuric acid ( $\text{H}_2\text{SO}_4$ , 98 %), nitric acid ( $\text{HNO}_3$ , 60 %) and isopropyl alcohol (IPA) were received from Daejung chemicals (Republic of Korea) and used as received. *m*-phenylenediamine (MPD, 99 %), trimesoyl chloride (TMC, 98 %), sodium hypochlorite ( $\text{NaOCl}$ , 10 – 13 %), 5,5-dimethyl-1-pyrroline-N-oxide (DMPO, for ESR analysis), and sodium chloride ( $\text{NaCl}$ , 99 %) were supplied from Aldrich and used without any purification. Deionized (DI) water was obtained from water purification system (Synergy, Millipore, USA), having a resistivity of 18.3  $\text{m}\Omega\text{ cm}$ . *n*-hexane (95 %) was received from Samchun Chemicals (Republic of Korea).

### 2.2 Preparation of CNT containing acid functional groups (CNTa)

The CNTs were modified using the acid mixture of sulfuric acid and nitric acid (3 : 1 volume ratio) to impart functional groups such as carboxylic acid. 0.2 g of raw CNTs was placed in the 250 mL of round-bottom flask with a magnetic stirring bar. The 90 mL of acid mixture solution was added into the flask. Then the flask was placed into the oil bath thermostated at 65 °C with stirring. After 4.5 h of reaction, the solution cooled to room temperature and diluted with 2.0 L of water. The diluted solution was filtered using anodic aluminium oxide (AAO) filter having 0.2  $\mu\text{m}$  of pore size. The filtered solid was washed by water until a neutral pH is attained. The resulting CNT (CNTa) was dried in the 35 °C vacuum oven.

### 2.3 Preparation of GOs

The graphene oxides (GOs) were prepared through the modified Hummers method.<sup>27, 36</sup> 1.5 g of graphite powders and 0.75 g of phosphorus pentoxide were placed into the 50 mL of round-bottom flask. 9.0 mL of sulfuric acid was added to the flask and the flask was placed into the oil bath thermostated at 85 °C. After 5 h of reaction, the reaction solution was diluted with 300 mL of water and filtered using AAO filter. The

filtrated solid was dried in the 35 °C vacuum oven over 12 h. 1.0 g of the dried solid (pre-oxidized graphite), 0.5 g of sodium nitrate, and 23 mL of sulfuric acid were placed into the 100 mL round-bottom flask with a magnetic stirring bar. The temperature was controlled at 0 °C by placing into the ice bath for 40 min without stirring. Then 3.0 g of potassium permanganate was carefully added into the flask and the mixture was heated to 35 °C with stirring. After 2 h, the solution was diluted with 140 mL of water and 10 mL of 30 % hydrogen peroxide. Then the mixture was centrifuged at 10000 rpm for 30 min. The settled solid was washed with ethanol and water, and then filtrated with AAO filter. The resulting solid, GO, was dried in the 35 °C vacuum oven.

### 2.4 Dispersity Evaluation

The maximum dispersity of CNTa and/or GO in water was evaluated using previous method reported by Park et al.<sup>37</sup> 500 mg of CNTa and/or GO were dispersed in 10 mL of water using bath sonicator for 1 h at room temperature. After dispersion, solution was left for 2 weeks and centrifuged for 30 min at 1000 rpm. The supernatant was filtered using weight-measured AAO filter. Then fully dried AAO filters with CNTa and/or GO were weighed, then the maximum dispersity value could be obtained by comparing the weights of the pristine AAO filter with that of the AAO filter with CNTa and/or GO.

### 2.5 Preparation of the Polyamide Membranes with/without carbon nanomaterials

The following procedure was used for the preparation of polyamide membrane without any carbon nanomaterials (PA membrane). Polysulfone (PSf) support membrane was treated with IPA for 10 min to activate pores and washed several times with water. The IPA-treated membrane was placed in the water bath for 3 h to stabilize the pores. The membrane was placed into the bath with 2 wt% aqueous solution of MPD. 0.1 wt% of TMC solution was prepared in *n*-hexane. After 3 h, the membrane was taken out and air bubble and droplet of aqueous solution on the membrane surfaces were removed carefully by air knife. The membrane was fixed on the acryl flat board with a rubber mold. The TMC solution was poured on the membrane saturated with aqueous solution. After 60 s of reaction, the excess of TMC solution was removed and the membrane was placed in the 100 °C oven for 5 min for crosslinking as well as further polymerization. The resulting membrane was washed with water several times. The polyamide membranes containing CNTa (PA-CNTa membranes), GO (PA-GO membranes), and the mixture of CNTa and GO (PA-CNTa/GO membranes) were prepared using the same procedure for PA membrane except the composition of aqueous solution containing 3 wt% of MPD and 0.0002 to 0.3 wt% of CNTa, GO, and CNTa/GO mixture in aqueous solution. All the membranes were prepared in the fume-hood at room temperature.

### 2.6 Membrane Filtration Test

Water flux and salt rejection values were measured by the lab-scale cross-flow RO membrane test unit. The effective membrane area was 3.3  $\times$  6.8  $\text{cm}^2$  with the 0.3 cm of channel height. The pressure was maintained at about 15.5 bar (225 psi) and the 2,000  $\text{mg L}^{-1}$  of NaCl solution was used as a feed solution (the conductivity of feed solution was about 3.84  $\text{mS cm}^{-1}$ ). Cross flow velocity at the membrane surface and the temperature were controlled to 500  $\text{mL min}^{-1}$  and 25 °C, respectively in the cross-flow system. This test condition has been generally used for measuring the performance of the BWRO membranes by others.<sup>10, 38-40</sup> Water flux was measured by weighing the permeate solution after the membranes were

compressed for 1 h at 15.5 bar. Water flux,  $J$ , was calculated using equation (1):

$$J = \Delta V / (A \times \Delta t) \quad (1)$$

where  $\Delta V$  is the volume of permeate collected between two weight measurements,  $A$  is the membrane surface area, and  $\Delta t$  is the time between two weight measurements.

Salt rejection was calculated using the following equation (2):

$$R = (1 - C_p / C_f) \times 100 \% \quad (2)$$

where  $R$  is salt rejection parameter,  $C_p$  is the salt concentration in permeate, and  $C_f$  is the salt concentration in feed. The salt concentrations were measured using conductivity meter (InoLab Cond 730P, WTW 82362, weilheim). All membrane performance results in this manuscript are the average values obtained by more than three measurements from the three membrane samples prepared at different times to confirm the reproducibility.

### 2.7 Characterizations

Morphologies of CNT and GO were observed by transmission electron microscopy (TEM, LIBRA 120, Carl Zeiss, Germany). 1 mg of CNT or GO was dispersed in 50 mL of water using sonication bath and then the dispersed solution was dropped on the TEM grid. The grid was dried in the 35 °C vacuum oven over 12 h. Raman spectroscopy (LabRam ARAMIS, Horiba Jobin-Yvon, France) was used to observe the damaged crystalline structure of CNT and GO surfaces. Raman spectroscopic mapping was carried out to observe the spatial distribution of CNT and GO in the polymeric membrane using the same device. Since fluorescences from PSf layer disturbs the detection of Raman scattering, thin active layer of membranes was transferred to silicon wafer. The excitation source was a diode laser with an excitation wavelength of 785 nm and a power of 5 mW. The laser excitation was focused using a 100× objective and the Stoke-shifted Raman scattering was recorded using a 1400/600 groove  $\text{min}^{-1}$  grating. Raman mapping image was collected within a  $10 \times 10 \mu\text{m}^2$  area of active layer of the membrane on silicon wafer. The Raman mapping image was obtained by integrating the area of characteristic peaks from polyamide, CNT, and GO. The surface compositions of the CNT and GO were analyzed by X-ray photoelectron microscopy (XPS, PHI-1600) using Mg K $\alpha$  (1254.0 eV) as radiation source. Survey spectra were collected over a range of 0–1100 eV, followed by high resolution scan of the C 1s and O 1s regions. The UV-Vis spectrum was measured by Agilent 8453 UV-Visible Spectrometer at room temperature. Zeta potential values of CNTa, GO, and the mixture of CNTa and GO dispersed solution were measured by electrophoretic light scattering spectrophotometer (ELS-8000) to investigate of colloidal stabilities. Highly concentrated solution, 50  $\text{mg mL}^{-1}$  of carbon nanomaterials dispersed in water, was used because the device has a limitation on detecting intensity. Fourier-transform infrared (FT-IR) spectra of CNT and GO were measured in transmission mode in the frequency range of 4000–650  $\text{cm}^{-1}$  on a Nicolet 6700 instrument (Thermo Scientific, USA). FT-IR spectra of dried membranes were recorded in attenuated total reflectance (ATR) mode in the frequency range of 4000–650  $\text{cm}^{-1}$  on a Nicolet 6700 instrument (Thermo Scientific, USA). The spectrum was collected as the average of 32 scans with the resolution of 8  $\text{cm}^{-1}$ . Each membrane sample was put in equal physical contact with sampling plate of the spectrometer accessory to avoid difference caused by pressure and/or penetration depth. Surface morphologies of the membranes were inspected by scanning

electron microscopy (SEM, JSM-6701F, JEOL) using a field emission scanning electron microscope (FESEM). The mechanical properties of the membranes were measured by universal tensile testing machine (UTM). The dumbbell specimens were prepared using the ASTM standard D638 (Type V specimens dog-bone shaped membrane samples). Thermal gravimetric analysis (TGA) was performed in a Q-5000 IR from TA Instruments, using a heating rate of 10 °C /min under the air atmosphere. The investigation of radical scavenging effect of the CNT and GO was performed using electron spin resonance (ESR) spectrometer (JEOL, JES-TE200). The production of free radicals from sodium hypochlorite was monitored in the presence of the spin trap agent DMPO. The membrane active layer was soaked in the solution containing sodium hypochlorite (500 ppm) and DMPO (2 ppm), and then the ESR spectrum was obtained in every 10 min.

## 3 Results and discussion

### 3.1 Preparation of CNT having acid functional groups (CNTa) and GO

Since the polyamide nanocomposite membranes are prepared by the interfacial polymerization reaction using the aqueous solution of MPD and the organic solution of TMC, CNT should be well-dispersed either in the aqueous solution or the *n*-hexane solution to be incorporated.<sup>41</sup> To disperse CNT in *n*-hexane, aliphatic hydrocarbon chains should be attached on CNT, while it needs several reaction steps with several purification procedures.<sup>42–44</sup> In contrast, if CNT is treated with strong acids by a one-step reaction, it could be well-dispersed in the aqueous solution.<sup>43</sup> Therefore, in present study, pristine CNT was modified using the strong acid mixture of sulfuric acid and nitric acid (volume ratio of 3 to 1) to prepare CNT with acidic functional groups (CNTa), following the procedure reported before.<sup>11, 43</sup> We previously found that when 1 g of CNT was reacted with 300 mL of the acid mixture at 65 °C for 4.5 h, it could be well-dispersed in the aqueous solution of MPD.

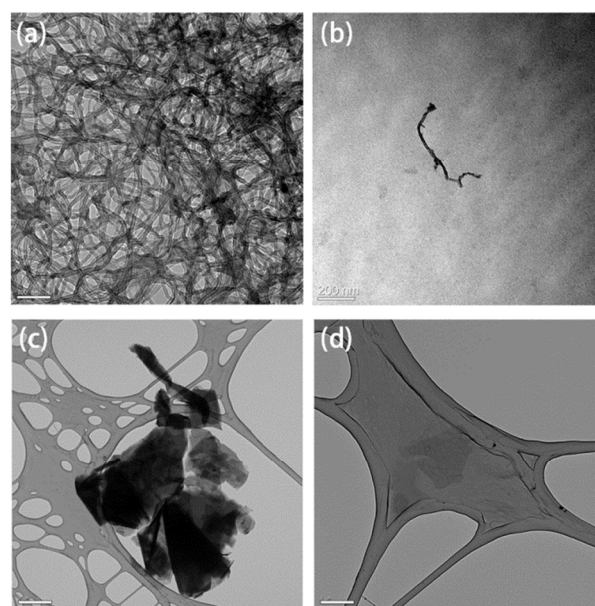


**Fig. 1** TEM images of (a) pristine CNT, (b) CNTa, (c) graphite, and (d) GO.

Consequently, when RO membrane was prepared using the aqueous solution containing 0.001 wt% of CNT, maximum membrane performance was obtained.<sup>11</sup> The successful incorporation of oxygen functional groups, such as carboxylic acid and hydroxyl groups into CNT through the modification process could be confirmed by XPS analysis, Raman spectroscopy, and FT-IR as shown in the Electronic Supplementary Information (ESI, Table S1, Fig. S1, S2, and S3†). CNT was also observed to become shorter, and the entanglements of the CNTs disappeared by the acid treatment process (Fig. 1a and b). GO was prepared to have oxygen functional groups, such as epoxy, carbonyl, hydroxyl, and carboxylic acid groups, by the modified Hummer's method.<sup>27,36</sup> The successful synthesis of GO was confirmed by XPS analysis, Raman spectroscopy, and FT-IR analysis (Table S1, Fig. S1, S2, and S3†). The TEM images in Fig. 1c and d show the thin layer structure of GO formed by the exfoliation of graphite. The dark-stacked structures are observed from graphite, while the light grey-planer image is observed from GOs demonstrating single or a few layers. The CNTa and GO having the oxygen functional groups are expected to be well-dispersed in the aqueous solutions as well as in the polyamide active layer due to the hydrogen-bonding and/or dipole-dipole interactions as reported before.<sup>11,45</sup>

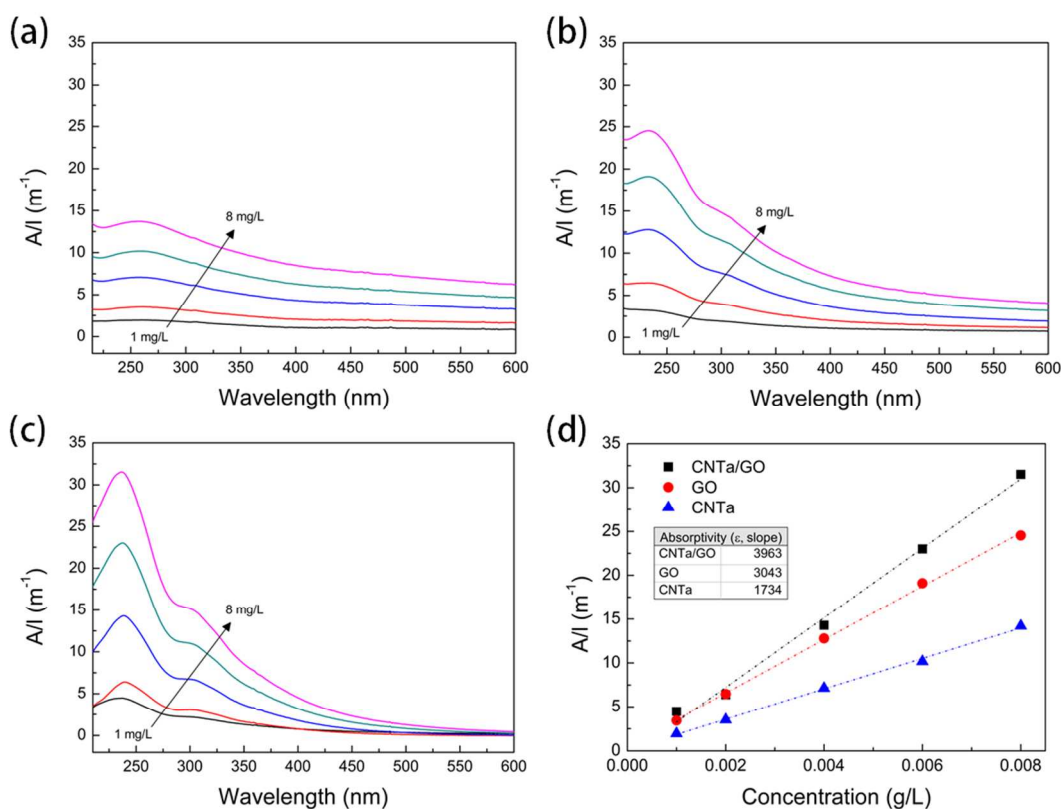
### 3.2 Dispersion Evaluation

Table 1 shows the maximum dispersity of the carbon nanomaterials in water. The maximum dispersity value of the CNTa/GO mixture was found to be larger than those of CNTa and GO in all cases. It is well known that the dispersion of CNT in the aqueous solution can be improved by adding GO because GO can work as a surfactant through the interactions with CNT

**Table 1** Maximum dispersity ( $\text{g L}^{-1}$ ) of CNTa, GO, and CNTa/GO mixture in water.

CNTa	GO	CNTa : GO mixture	
		1:9	30.7 ± 3.8
		3:7	33.1 ± 2.2
16.2 ± 2.0	19.7 ± 2.5	5:5	22.0 ± 6.2
		7:3	35.5 ± 3.9
		9:1	28.5 ± 4.3

by hydrogen bonding,  $\pi$ - $\pi$  interactions, and van der Waals forces.<sup>30,33,34</sup> In addition, when CNTa and GO co-existed in the aqueous solution, the individual formation of the tubular bundled structure of CNTs and the sheet-stacked structure of GOs could be disturbed by forming multi-dimensional nanostructures.<sup>32</sup> Since the CNTa/GO mixture in 7 to 3 (CNTa to GO) ratio showed the largest maximum dispersity value, it was used for further dispersity analysis and the preparation of PA-CNTa/GO membranes. Previous studies also reported that the mixture showed the highest dispersity behavior when the CNT to GO ratio of 2 to 1 was used, because thermodynamically stable structures could be formed at that ratio.<sup>33</sup>



**Fig. 2** UV/vis absorption spectra of (a) CNTa, (a) GO, and (c) CNTa/GO dispersed aqueous solution and (d) their UV/vis absorption intensity changes by the concentration.

For quantitative analysis of the dispersion behavior, UV-Vis absorbance spectroscopy of CNTa, GO, and CNTa/GO dispersed solution was observed, as shown in Fig. 2a to c. The absorptions observed at 230 and 300 nm could be ascribed to the  $\pi-\pi^*$  transition and  $n-\pi^*$  transition, respectively. The absorption intensity at 230 nm was found to be larger than that at 300 nm because the electron transition from  $\pi$  to  $\pi^*$  is much more predominant than that from  $n$  to  $\pi^*$  in most compounds.<sup>37</sup> Therefore, the 230 nm peak showing the maximum intensity can be assigned as  $\lambda_{\max}$ . The intensity of  $\lambda_{\max}$  at 230 nm of the CNTa/GO mixture was found to be larger than those of CNTa and GO individually, indicating that the CNTa/GO mixture is more well-dispersed in the aqueous solution than the solutions containing CNTa or GO only. The changes in absorption intensity at different concentrations are shown in Fig. 2d, for which the slope could be assigned to the absorptivity ( $\epsilon$ ) in the Beer-Lambert law ( $A = \epsilon l c$ ), where  $A$  is the measured absorbance,  $\epsilon$  is the absorptivity,  $l$  is the path length of UV-Vis light, and  $c$  is the solution concentration. As expected, CNTa/GO showed the largest absorptivity ( $\epsilon$ ) value, and the very large absorptivity value has been known to indicate the excellent dispersion of the carbon nanomaterial.<sup>37</sup>

Fig. 3 shows the zeta potential behavior of the carbon nanomaterials (500 mg in 10 mL) used in this study. Zeta potential values have been correlated with the colloidal stability of the particles in water; potentials of  $\pm 10$  to  $\pm 30$ ,  $\pm 30$  to  $\pm 40$ ,  $\pm 40$  to  $\pm 60$ , and  $> \pm 60$  mV have been assigned to indicate incipient, moderate, good, and excellent stable colloidal states, respectively.<sup>46,60</sup> Therefore, the zeta potential values of CNTa, GO, and the CNTa/GO mixture of about  $-36 \pm 6.2$  mV,  $-58 \pm 7.5$  mV, and  $-60 \pm 9.5$  mV, respectively, can be assigned to the moderate, good, and excellent stable states, respectively. Negative zeta potentials were observed due to the oxygen functional groups of carbon nanomaterials in this study. In addition to the maximum dispersity and UV-vis spectroscopy studies, the zeta potential behavior also indicated that CNTa/GO shows much better dispersion in water than CNTa or GO only. Since the CNTa/GO mixture is more well-dispersed in the aqueous solution than CNTa and GO alone in the solutions, it is expected that there are less amount of aggregated particles in the CNTa/GO solution than CNTa and GO solutions. Then CNTa/GO should have the larger surface area and smaller particle size than CNTa and GO, resulting in large zeta potential value of CNTa/GO solution. In this regard, it is also very possible that CNTa/GO would be more well-dispersed

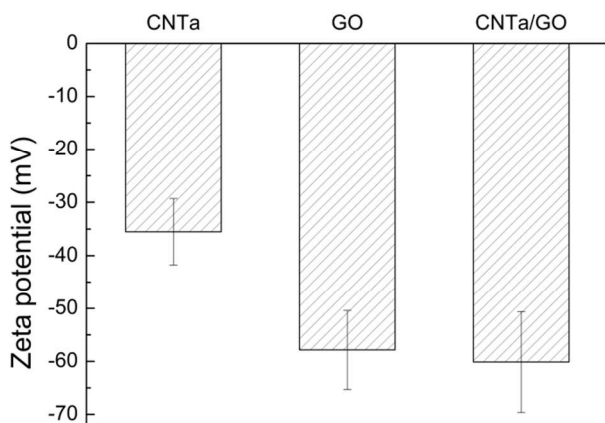


**Fig. 3** Zeta potential values of CNTa, GO, and CNTa/GO dispersed in water ( $50 \text{ mg mL}^{-1}$ ).

in the polyamide active layer in the membrane because the polyamide layer is prepared from interfacial polymerization using the MPD aqueous solution containing the carbon nanomaterials. The state of CNTa/GO in the polyamide matrix could be confirmed to be well-dispersed or aggregated by the SEM, TEM and Raman studies, shown in the next part of this manuscript.

### 3.3 Preparation of polyamide membranes with/without the carbon nanomaterials

PA, PA-CNTa, PA-GO, and PA-CNTa/GO membranes were prepared by the typical interfacial polymerization method used for the preparation of other RO membranes except that CNTa, GO, or CNTa/GO was included in the MPD aqueous solution. The PA membrane was prepared using 2 wt% MPD aqueous solution without any carbon nanomaterials. The PA-CNTa, PA-GO, and PA-CNTa/GO membranes were prepared using 3 wt% MPD aqueous solution as this concentration showed maximum water flux and salt rejection values, while the PA membrane showed optimal performances at 2 wt% MPD aqueous solution (Table S2†). Previously, 2 and 3 wt% of MPD were also found to be the optimized concentrations to obtain high-water flux PA and PA-CNTa membranes, respectively.<sup>11</sup> It is generally accepted that the monomer ratio for interfacial polymerization could determine the cross-linking density, polarity, and polymer structure, which affect the membrane performances.<sup>40,47</sup> It is also possible that the oxygen functional groups on CNTa and GO could form salt structures and/or hydrogen bonding with amine groups of MPD during the interfacial polymerization. Then, a slightly larger amount of MPD would be needed to prepare the polyamide membranes with carbon nanomaterials to allow maximum water flux and salt rejection properties due to complexing of some of the amine groups of MPD with the functional groups of CNTa and GO.

The formation of the polyamide active layer was confirmed by FT-IR analysis (Fig. S4†). Characteristic peaks from the polyamide structures were observed at  $1540 \text{ cm}^{-1}$  (N-H bend),  $1608 \text{ cm}^{-1}$  (NH-CO vibration), and  $3397 \text{ cm}^{-1}$  (O-H and N-H stretch) for the PA, PA-CNT, PA-GO, and PA-CNT/GO membranes. The characteristic peaks from the carbon nanomaterials could not be clearly detected because their content in the polyamide layers are too small; In the 3 wt% MPD aqueous solutions only 0.0002 to 0.03 wt% of carbon nanomaterials were used, making the content of carbon nanomaterials in the polyamide layer smaller than 1.0 wt%.

The morphologies of the PA and PA-CNTa/GO membranes and the dispersion of CNTa/GO in the polyamide active layer were observed by SEM and TEM. Fig. 4a shows the SEM images of the top surface of the PA membrane. The typical ridge-and-valley structures were observed, indicating the successful formation of polyamide active layer. Since the densities of CNT and GO are larger than water, most of the mixtures of CNTa and GO sank into the bottom/inner part of the active layer during the membrane preparation procedure. Therefore, only a small amount of CNTa/GO was observed on the top surface of the PA-CNT/GO membrane (Fig. 4b). The embedment of CNTa and GO at the inner/bottom part of the active layer was confirmed by SEM images taken of the bottom part and cross-sectional TEM images. Fig 4c and d show SEM images of the bottom part of the active layers of PA and PA-CNTa/GO membranes. Clear and flat images were observed for the PA membrane, while protruding domains with linear and planer shapes were observed in the PA-CNTa/GO membrane. The linear and planer images should originate from the tubular

structures of CNT and the planer sheet structures of GO, respectively. The embedment of CNTa/GO in the polymer matrix could be also observed from the cross-sectional TEM images, as shown in the Fig. S5†. It was very clear that PA membrane did not have any dark images from the carbon nanomaterials within the polyamide layer, which was about 200 nm thick, while dark images originating from CNTa and GO were observed in the PA-CNTa/GO membrane. When the PA-CNTa and PA-GO membranes were prepared using 0.005 wt% or smaller concentrations of CNTa and GO in the aqueous solution, respectively, CNTa and GO were found to be well-dispersed in the polyamide layers. However, large clusters over 5  $\mu\text{m}$  in size were observed in the SEM images when concentration larger than 0.005 wt% was used (Fig. S6†). Therefore, 0.005 wt% should be the maximum concentration for the preparation of the PA-CNTa and PA-GO membranes with good dispersion of the carbon nanomaterials. This could be also confirmed from the membrane performance results. In addition, any coagulated clusters by the CNTa and GO were not observed from the PA-CNTa/GO membranes when the CNTa/GO concentration in the aqueous solution was 0.02 wt% or smaller, while some clusters larger than 5  $\mu\text{m}$  were observed when 0.03 wt% of CNTa/GO was used (Fig. S6†). Therefore, 0.02 wt% might be the maximum concentration for the preparation of the membrane having the CNTa/GO with well-dispersed state, which could be further confirmed from the membrane performance behavior shown in the later part of this

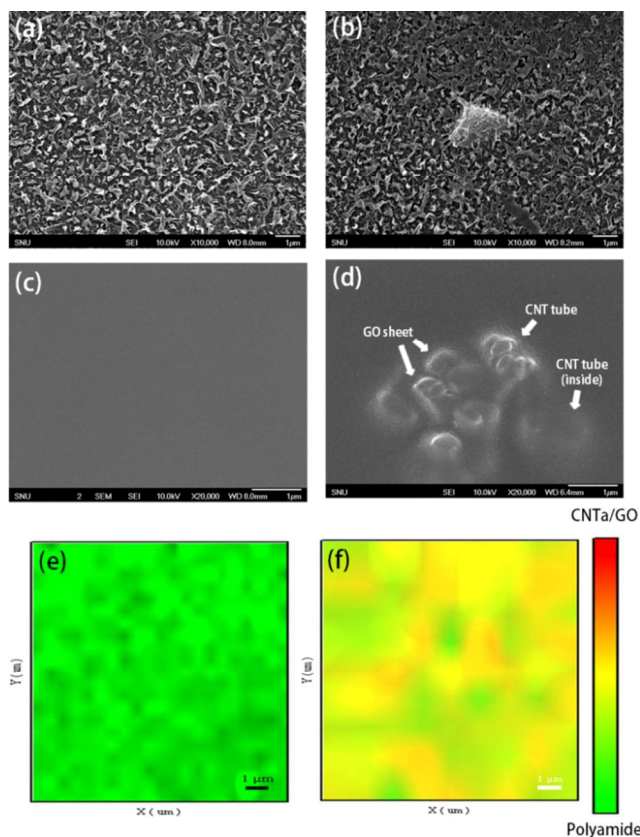


**Fig. 4** SEM (top and bottom part) and Raman spectroscopic mapping images of (a), (c), (e) PA, and (b), (d), (f) PA-CNTa/GO (prepared using the MPD aqueous solution containing 0.02 wt% of CNTa/GO) membranes.

manuscript. The differences in the maximum concentration demonstrating the good dispersion of the carbon nanomaterials in the membranes could be correlated with the dispersity behavior of CNTa, GO, and CNTa/GO in the aqueous solution. The CNTa/GO with better dispersion in water can be dispersed in the polyamide active layer better than the less dispersed CNTa or GO.

Since the amount of CNTa/GO in the polyamide was too small, it was not possible to observe the overall distribution of CNTa/GO in the nanocomposite membranes through SEM or TEM. Therefore, Raman spectroscopic mapping was carried out for further confirmation of the spatial distribution of CNT/GO in the polyamide membranes. Raman spectroscopic mapping has been used as a tool to visualize the spatial distribution of nanomaterials in other matrix materials including polymers.<sup>11, 48-50</sup> Raman spectroscopic mapping images of the PA and PA-CNT/GO membranes are shown in Fig. 4e and f, respectively. The characteristic peaks of polyamide, the D band, and G band of CNTa and GO were observed at 998  $\text{cm}^{-1}$ , 1308  $\text{cm}^{-1}$  and 1600  $\text{cm}^{-1}$ , respectively, and mapping images were obtained by integrating the region of those characteristic peaks. The green and red colors represent the polyamide and CNTa/GO structures, respectively. Only green color was observed in Fig. 4e, while well-dispersed images of green and red colors and even yellow color were observed from the Raman mapping image of the PA-CNT/GO membrane, indicating that CNT and GO were well-incorporated and -dispersed in the polyamide layers.

### 3.4 Water flux and salt rejection

The water flux and salt rejection of the membranes were measured by lab-scale cross-flow equipment for possible practical application in RO systems. The water flux and salt rejection values of PA membrane measured in this study were  $34.00 \pm 0.67$  LMH and  $96.63 \pm 1.34$  %, respectively. These values were close to those of RO membranes having polyamide active layer, previously reported by others.<sup>10,47,51</sup> In addition, the LFC-1 membrane, a commercial membrane for brackish water filtration, was tested at the same operating condition for comparison. The water flux and salt rejection values of the LFC-1 membrane were  $37.75 \pm 1.5$  LMH and  $97.01 \pm 0.8$  %, respectively, which are smaller than those in the technical specification supplied by the company. Such discrepancy has been reported by others due to the effect of the membrane filtration conditions.<sup>61</sup> It is also well known that various additives and post treatment are used to prepare the polyamide active layers of commercial membranes, which can increase the membrane performances. For this reason, the water flux and salt rejection values of our PA membrane were smaller than those of the LFC-1 membrane. However, the differences were not large, and the main objective of this manuscript is to investigate the effect of CNTa/GO in the active layer. Therefore, any additives and post treatments were intentionally not used for membrane preparation, and their membrane performance behaviors were compared.

Fig. 5 shows the water flux and salt rejection values of the membranes. When the PA-CNTa and PA-GO membranes were prepared with very small amounts of CNTa and GO, respectively (0.0002 wt% in aqueous solution), the water flux and salt rejection values were almost the same as those of the PA membrane because the amounts in the polyamide matrix were too small to affect the membrane performances. The PA-CNTa and PA-GO membranes prepared using 0.001 to 0.005 wt% of CNTa and GO in aqueous solution, respectively, showed increased water flux values without much decrease of

the salt rejection. When PA-CNTa and PA-GO membrane were prepared using larger than 0.005 wt% of CNTa and GO, respectively, the water flux increased while the salt rejection decreased dramatically, possibly due to the formation of large voids caused by the aggregation of the carbon nanomaterials. The aggregated structures were observed by SEM (Fig. S6†), working as defects in the membranes, and they could provide the large passage ways for the water and ion molecules. The maximum water flux values of the PA-CNTa and PA-GO membranes maintaining high enough salt rejection were larger

than that of PA membrane by 9.45 LMH (27.2 % increase) and 6.21 LMH (17.8 % increase), respectively, while the differences of salt rejection values were smaller than 0.1 %. The increase of water flux could be explained by the water transportation mechanisms of CNT and GO, as described in previous researches.<sup>11,20,21,23,52,53</sup> Water molecules can enter the CNT nano-channel by capillary force and go through quickly due to the hydrophobic inner side of CNT. Thus, the possible passage of water molecules through the polyamide matrix could be shortened, resulting in the increase of water permeability.

The graphitic sheet structures have been known to increase the water permeability because the hydrated ions can go through the CNT nano-channel and on the surface of CNT and GO easily by surface transporting or nano-channel mechanism. The increase of the water flux did not decrease the salt rejection because the carbon nano-materials are well-dispersed in the continuous polyamide matrix without any defects larger than the size of the sodium or chloride ions in the hydrate state.

The water flux values of the PA-CNTa/GO membranes were found to increase with increase of the CNTa/GO concentration up to 0.02 wt% maintaining reasonably high salt rejection value; the changes of the salt rejection values were less than 0.8 %. However, when the concentration became larger than 0.03 wt%, water flux increased while there was a dramatic decrease of the salt rejection for the same reason as the PA-CNTa and PA-GO membranes. Still, the 0.02 wt% maintaining a reasonably high salt rejection value for PA-CNTa/GO membrane was much larger than 0.005 wt% for the PA-CNTa and PA-GO membranes. The maximum water flux of the PA-CNTa/GO membrane maintaining a reasonably high salt rejection value was larger than that of the PA membrane by 73.41 %. Therefore, the best membrane performance in terms of the water flux and salt rejection was observed from the PA-CNTa (44.23 LMH and 96.75 %), PA-GO (39.19 LMH and 96.97 %), and PA-CNTa/GO (58.96 LMH and 96.21 %) membranes prepared using 0.001, 0.001, and 0.02 wt% of the carbon nanomaterials in MPD aqueous solution, respectively. Accordingly, these were used for further the stability and durability studies shown in the following part.

Fig. 6 shows the water permeability (unit water flux, the water flux per applied pressure) behavior of the membranes with different applied pressure. The water permeability has been known to decrease with the increase of applied pressure because the polymer layers are compressed by the pressure, causing water transport channels to become smaller. Therefore, the PA membrane composed of only polymer without any filler showed the decrease of the water permeability with increasing applied pressure. However, the PA membranes containing carbon nanomaterials showed the increase of the water permeability value with increase of the pressure, indicating that larger amounts of water molecules passes through the surface of CNTa and/or GO or even inside of CNTa by overcoming the approach and entry resistance due to kinetic energy from the increased pressure.<sup>23</sup> Especially, the larger increase of the flux was observed for the PA-CNTa and PA-CNTa/GO membranes than for the PA-GO membrane indicating that the channel structures of CNTa increase the flux more than the flat GO structure. Possibly, flat GO structure might prevent the water molecule to go into the inside channel of the CNTs by wrapping the tube structures. However, such morphology could not be observed from the TEM or SEM images due to the limited resolution of the equipment. The effect of the applied pressure on salt rejection was also measured to estimate membrane stability (Fig. S8†). Salt rejection value was found to

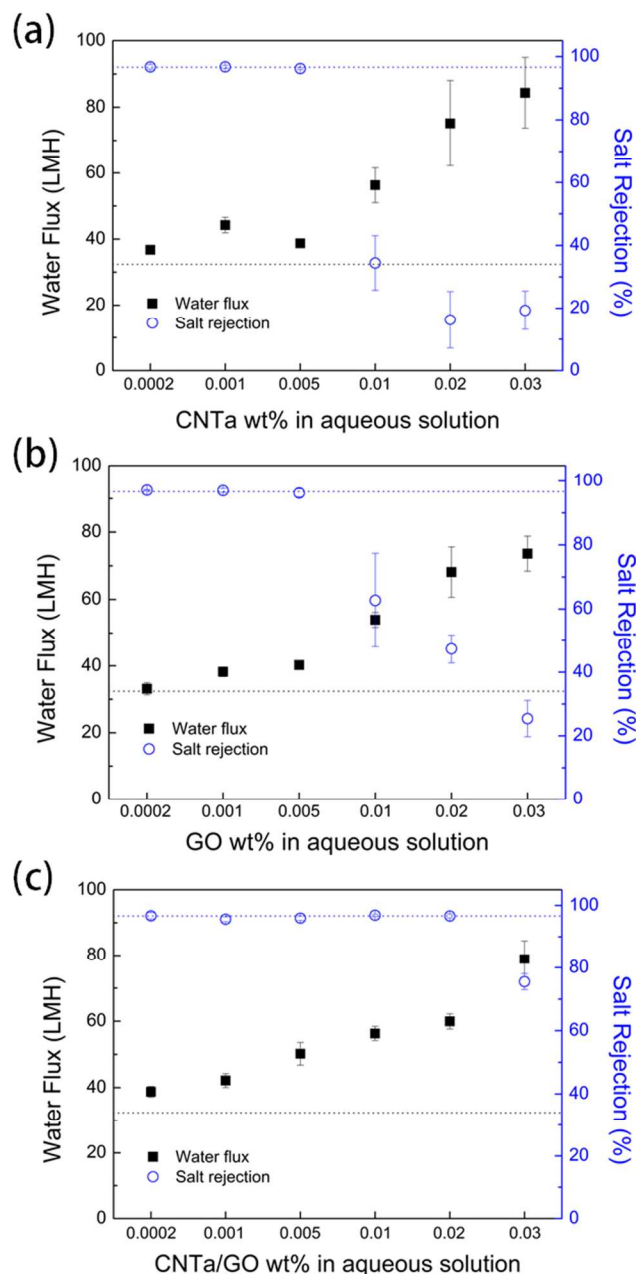


**Fig. 5** Water flux and salt rejection of (a) PA-CNTa, (b) PA-GO, and (c) PA-CNTa/GO membranes (water flux and salt rejection values of PA membrane were marked with black and blue dot lines, respectively) (tested by cross-flow filtration, 2000 ppm NaCl solution as a feed solution, 15.5 bar of feed pressure, and 500 mL min<sup>-1</sup> of flow rate).

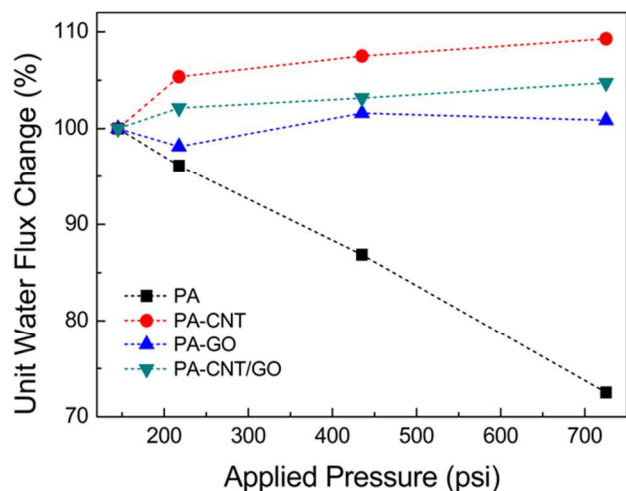


**Fig. 6** Unit water flux changes of PA, PA-CNTa (prepared using the MPD aqueous solution containing 0.001 wt% of CNTa), PA-GO (prepared using the MPD aqueous solution containing 0.001 wt% of GO), and PA-CNTa/GO (prepared using the MPD aqueous solution containing 0.02 wt% of CNTa/GO) membranes under different applied feed pressure (tested by cross flow filtration, 2000 ppm NaCl solution as a feed solution, and 500 mL min<sup>-1</sup> of flow rate).

increase slightly with the increase of applied pressure for all the membranes because to the formation of the compressed active layer by the pressure.<sup>59</sup> We believe that the detailed information of nanostructures of the CNTa/GO mixture should be very important to understand these membrane performance behavior of the PA-CNTa/GO membrane, while the observation and explanation of CNTa/GO nanostructure should need a serious of efforts and are beyond the scope of this study.

### 3.5 Durability of the PA-CNTa/GO membrane

Fig. 7a shows the pure water flux of the membranes measured with time. The water flux of the PA membrane decreased by 35.5 % after 72 h, whereas those of the PA-CNTa, PA-GO, and PA-CNTa/GO membranes decreased by only 24.8, 23.1, and 15.0 %, respectively, when the filtration test was performed at 15.5 bar of applied pressure. Similar flux decline behavior was observed when the feed pressure was increased to 50.0 bar; 37.5, 27.2, 23.8, and 16.2 % of water flux decreases were observed from PA, PA-CNTa, PA-GO, and PA-CNTa/GO membranes, respectively (see ESI, Fig. S9†). The decrease of water flux with time has been ascribed to membrane compression by the pressure.<sup>11, 23, 24</sup> The smaller flux decrease of the PA membranes with the carbon nanomaterials should be originated from the increase of mechanical strength. It is well known that one of the most important advantages of using CNT and GO as filler materials in the polymer matrix is the increase of physical properties including mechanical strength, because the fillers can disturb the polymer chain mobility to form stiffer polymer structures.<sup>28, 31, 33, 54</sup> Therefore, the polyamide active layers of the PA membranes with the carbon nanomaterials can be compressed less than that of the PA membrane, which in turns the smaller decrease of water flux. In addition, since the amount of CNTa/GO in the PA-CNTa/GO membrane is larger than those in the PA-CNTa and PA-GO membranes, the decrease of flux was found to be smaller for the PA-CNTa/GO membrane than the PA-CNTa and PA-GO membranes. The same behaviour was observed from the membrane durability test using the NaCl solution as shown in Fig. 7b. The increase

of mechanical strength producing the increase of durability upon long time operation could be confirmed by Young's modulus and tensile strength values of the membranes (see ESI, Fig. S10†). The Young's modulus and the tensile strength values of the PA membranes with the carbon nanomaterials were larger than those of the PA membrane without the carbon nanomaterials, and the PA-CNTa/GO membranes showed the largest values because it contained the largest amount of the carbon nanomaterials. Comparing the PA membranes prepared with the same concentration of the carbon nanomaterials (0.001 wt% of CNTa, GO, and CNTa/GO in the aqueous solutions, respectively), the mechanical property values were in the orders of PA-CNTa < PA-GO < PA-CNTa/GO, although the differences are not large. The mechanical strength behavior followed the maximum dispersity behavior shown in Table 1. Obviously, the carbon nanomaterials with better dispersity in the polymer matrix can increase the mechanical strength more.<sup>30-32</sup>

Disinfection has been widely used in RO process to prevent biofilm formation because biofilms formed on the membrane surfaces decreases the membrane performance dramatically which in turn increases the operation costs. Chlorine is

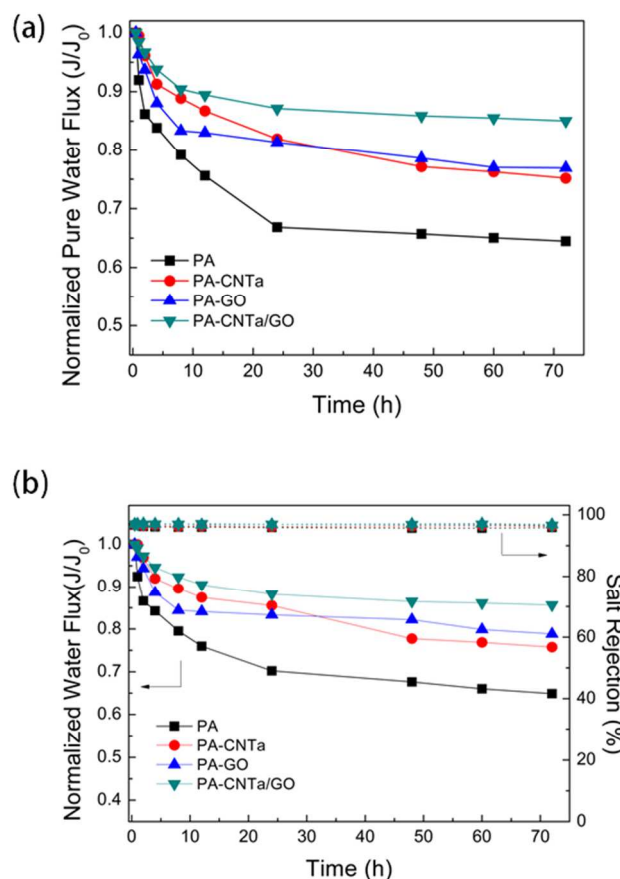


**Fig. 7** (a) Pure water flux measurement and (b) water flux and salt rejection behaviors with time for PA, PA-CNTa (prepared using the MPD aqueous solution containing 0.001 wt% of CNTa), PA-GO (prepared using the MPD aqueous solution containing 0.001 wt% of GO), and PA-CNTa/GO (prepared using the MPD aqueous solution containing 0.02 wt% of CNTa/GO) membranes (tested by cross-flow filtration, 2000 ppm NaCl solution as a feed solution, 15.5 bar of feed pressure, and 500 mL min<sup>-1</sup> of flow rate).

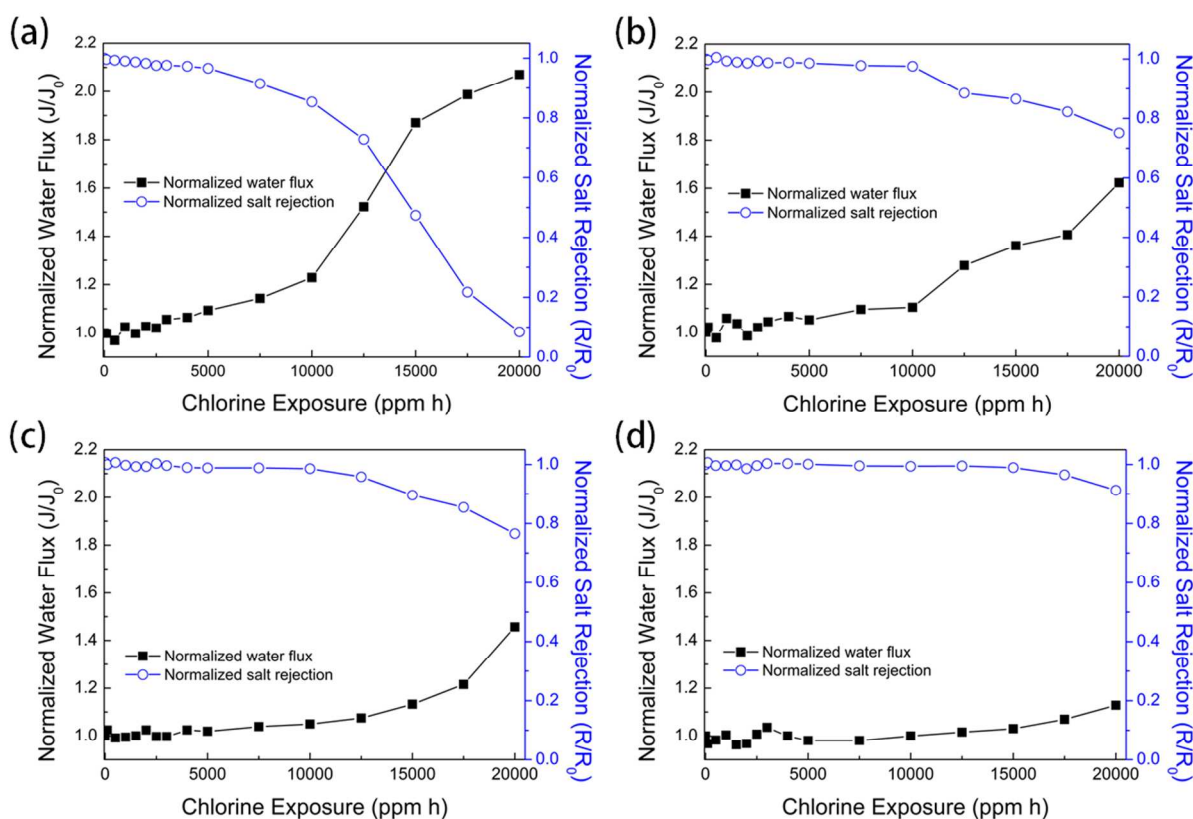


**Fig. 8** Membrane performance behaviors under the active chlorine exposures; (a) PA, (b) PA-CNTa (prepared using the MPD aqueous solution containing 0.001 wt% of CNTa), (c) PA-GO (prepared using the MPD aqueous solution containing 0.001 wt% of GO), and (d) PA-CNTa/GO (prepared using the MPD aqueous solution containing 0.02 wt% of CNTa/GO) membranes (tested by cross-flow filtration, measured after the chlorine exposure using 500 ppm chlorine solution, 2000 ppm NaCl solution as a feed solution, 15.5 bar of feed pressure, and 500 mL min<sup>-1</sup> of flow rate).

commonly applied as an oxidizing biocide for the disinfection process because of its low-cost and high-efficiency.<sup>9, 55, 56</sup> However, polyamide membranes have been known to have poor resistance to oxidizing agents including chlorine.<sup>9, 56, 57</sup> Fig. 8 shows the membrane performance behaviors under the active chlorine exposures. NaCl rejection of the PA membrane decreased by 8.55 % after only 7,500 ppm h (15 h) of chlorine exposure, falling off rapidly thereafter. After 40 h of chlorine exposure (20,000 ppm h), rejection ability of the PA membrane was not observed. In contrast, a smaller decrease of the salt rejection was observed from PA membranes with the carbon nanomaterials. Amide groups in polyamide layers can be attacked by oxidation reagents, such as the chlorine radical, hydroxyl radical, and hypochlorite (Fig. S11†). For example, since the hydroxyl radical is even smaller than the water molecule it can diffuse into the polyamide active layer easily and degrade the polymer structures. CNTa and GO in the polymer matrix can trap the radicals because they have the phenolic moieties having the radical scavenging ability.<sup>14, 28, 58</sup> Therefore, the inclusion of CNTa and GO in the polyamide active layer can increase the chlorine resistance of the membranes. The chlorine resistance ability of the PA-GO membrane was found to be slightly larger than that of the PA-CNTa membrane, indicating that GO is more effective to impart the chlorine resistance properties into membranes than CNT. In addition, the PA-CNTa/GO membrane showed the lower decreases in rejection than the PA-CNTa and PA-GO membranes due to the larger amounts of CNTa and GO in the

polyamide active layer. The other PA-CNTa/GO membrane intentionally prepared with the same amount of CNTa/GO (0.001 wt% in aqueous solution) showed the similar chlorine resistance behavior to the PA-CNTa and PA-GO membranes (Fig. S12†). Therefore, the chlorine resistance properties of the membranes with carbon nanomaterials should be mainly determined by the amount of carbon nanomaterials having the radical scavenging ability in the membranes, not much by the dispersity. The antioxidant effects (radical scavenging ability) of the carbon nanomaterials were further studied by TGA analysis under air, as reported by others (Fig. S13†).<sup>14, 58</sup> For the TGA study, the active layers were pulled off from the membranes and fully dried to remove the water for the accurate analysis. The antioxidant effect of the CNTa/GO was clearly demonstrated by the higher degradation temperature (such as onset temperature) of the active layer the onset temperature ( $T_d$ , 5% weight loss occurs) behavior agreed well with the chlorine resistance properties. The  $T_d$  values of the active layers of PA, PA-CNTa, PA-GO, and PA-CNTa/GO membranes were found to be 65.8, 73.3, 76.6, and 86.2 °C, respectively. The PA-CNTa/GO membrane showed the highest  $T_d$  because it contained the largest amount of carbon nanomaterials. The radical scavenging abilities of the carbon nanomaterials were further studied by ESR spectroscopy recorded during the active chlorine exposure to membrane active layers (see ESI, Fig. S14 and S15†) and the PA-CNTa/GO membrane was observed to have the best radical scavenging ability, which also agreed well with the TGA results.

## Conclusions

The polyamide membranes containing acid functionalized CNT (CNTa) and/or graphene oxide (GO) showed much improved performances such as the water flux, mechanical strength, durability, chlorine resistance, and the radical scavenging ability compared with the polyamide membrane without any carbon nanomaterials due the unique characteristics of the carbon nanomaterials. Especially, when the mixtures of CNTa and GO were used as the filler materials for the preparation of the membranes, much larger amounts of the carbon nanomaterials could be well-dispersed in the polymer layers than when CNTa or GO was used by alone, because GO can increase the dispersion of CNT in the aqueous solutions and the polymer matrix. Therefore, the polyamide membrane containing the mixture of CNTa and GO showed the best membrane performances. This result will undoubtedly contribute to the latest efforts to develop the polymer nanocomposites as well as the RO membranes without any trade off behaviors.

## Acknowledgements

This research was supported by the National Research Foundation of Korea Grant funded by the Korean Government (NRF-2010-C1AAA01-0029061) and Basic Science Research Program through the National Research Foundation (NRF-2013R1A1A2008607).

## Notes

School of Chemical and Biological Engineering and Institute of Chemical Processes, Seoul National University, 599 Gwanak-ro, Gwanak-gu, Seoul 151-742, Republic of Korea. Fax: +82-02-880-1604; Tel: +82-02-880-7070; E-mail: jongchan@snu.ac.kr

† Electronic Supplementary Information (ESI) available: Additional tables and figures; XPS elemental composition (at%) and O/C ratio of pristine CNT, CNTa, graphite, and GO (Table S1), water flux and salt rejection values of the membranes prepared in 2 and 3 wt% of MPD (Table S2), XPS spectra of pristine CNT, CNTa, graphite, and GO (Fig. S1), Raman spectra of pristine CNT, CNTa, graphite, and GO (Fig. S2), FT-IR spectra of pristine CNT, CNTa, graphite, and GO (Fig. S3), FT-IR spectra of PSf, PA, PA-CNTa, PA-GO, and PA-CNTa/GO membranes (Fig. S4), cross-sectional TEM images of PA and PA-CNTa/GO membranes (Fig. S5), coagulated structures from SEM images of PA-CNTa, PA-GO, and PA-CNTa/GO membranes (Fig. S6), contact angle values of PA, PA-CNTa, PA-GO, and PA-CNTa/GO membranes (Fig. S7), salt rejection measurement of PA-CNTa, PA-GO, and PA-CNTa/GO membranes at different applied pressure (Fig. S8), normalized pure water flux measurement with time at 50 bar of feed pressure for PA, PA-CNTa, PA-GO, and PA-CNTa/GO membranes (Fig. S9), mechanical properties of PA, PA-CNTa, PA-GO, PA-CNTa/GO membranes (Fig. S10), typical chlorination of polyamide membrane and antioxidant mechanism of CNT and GO (Fig. S11), Effect of chlorine exposure on the performances of PA-CNTa/GO membrane prepared using the MPD aqueous solution containing 0.001 wt% of CNTa/GO (Fig. S12), TGA analysis of active layers from PA, PA-CNTa, PA-GO, PA-CNTa/GO membranes (Fig. S13), ESR spectra obtained during the active chlorine exposure to membrane active layers from PA, PA-CNTa, PA-GO, PA-CNTa/GO membranes (Fig. S14), and time-dependent relative ESR intensity changes during the active chlorine exposure to membrane active layers from PA, PA-CNTa, PA-GO, PA-CNTa/GO membranes (Fig. S15). See DOI: 10.1039/b000000x/

## References

- 1 D. G. Kim, H. Kang, S. Han, H. J. Kim and J. C. Lee, *RSC Adv*, 2013, **3**, 18071-18081.
- 2 D. G. Kim, H. Kang, Y. S. Choi, S. Han and J. C. Lee, *Polym. Chem.-UK*, 2013, **4**, 5065-5073.

- 3 D. G. Kim, H. Kang, S. Han and J. C. Lee, *ACS Appl. Mater. Interfaces*, 2012, **4**, 5898-5906.
- 4 D. G. Kim, H. Kang, S. Han and J. C. Lee, *J. Mater. Chem.*, 2012, **22**, 8654-8661.
- 5 L. F. Greenlee, D. F. Lawler, B. D. Freeman, B. Marrot and P. Moulin, *Water Res.*, 2009, **43**, 2317-2348.
- 6 M. Elimelech and W. A. Phillip, *Science*, 2011, **333**, 712-717.
- 7 G. D. Kang and Y. M. Cao, *Water Res.*, 2012, **46**, 584-600.
- 8 D. Li and H. T. Wang, *J. Mater. Chem.*, 2010, **20**, 4551-4566.
- 9 H. B. Park, B. D. Freeman, Z. B. Zhang, M. Sankir and J. E. McGrath, *Angew. Chem. Int. Edit.*, 2008, **47**, 6019-6024.
- 10 H. Y. Zhao, S. Qiu, L. G. Wu, L. Zhang, H. L. Chen and C. J. Gao, *J. Membr. Sci.*, 2014, **450**, 249-256.
- 11 H. J. Kim, K. Choi, Y. Baek, D.-G. Kim, J. Shim, J. Yoon and J.-C. Lee, *ACS Appl. Mater. Interfaces*, 2014, **6**, 2819-2829.
- 12 M. Fathizadeh, A. Aroujalian and A. Raisi, *J. Membr. Sci.*, 2011, **375**, 88-95.
- 13 H. J. Kim, Y. Baek, K. Choi, D. G. Kim, H. Kang, Y. S. Choi, J. Yoon and J. C. Lee, *RSC Adv.*, 2014, **4**, 32802-32810.
- 14 P. C. P. Watts, P. K. Fearon, W. K. Hsu, N. C. Billingham, H. W. Kroto and D. R. M. Walton, *J. Mater. Chem.*, 2003, **13**, 491-495.
- 15 H. Im and J. Kim, *Carbon*, 2012, **50**, 5429-5440.
- 16 Q. F. Cheng, J. W. Bao, J. Park, Z. Y. Liang, C. Zhang and B. Wang, *Adv. Func. Mater.*, 2009, **19**, 3219-3225.
- 17 W. H. Guo, C. Liu, X. M. Sun, Z. B. Yang, H. G. Kia and H. S. Peng, *J. Mater. Chem.*, 2012, **22**, 903-908.
- 18 S. Kang, M. Herzberg, D. F. Rodrigues and M. Elimelech, *Langmuir*, 2008, **24**, 6409-6413.
- 19 D. R. Paul, *Science*, 2012, **335**, 413-414.
- 20 J. K. Holt, H. G. Park, Y. M. Wang, M. Stadermann, A. B. Artyukhin, C. P. Grigoropoulos, A. Noy and O. Bakajin, *Science*, 2006, **312**, 1034-1037.
- 21 G. Hummer, J. C. Rasaiah and J. P. Noworyta, *Nature*, 2001, **414**, 188-190.
- 22 J. N. Shen, C. C. Yu, H. M. Ruan, C. J. Gao and B. Van der Bruggen, *J. Membr. Sci.*, 2013, **442**, 18-26.
- 23 H. D. Lee, H. Y. Kim, Y. H. Cho and P. H. B., *Small*, 2014, **10**, 2653-2660.
- 24 V. Vatanpour, S. S. Madaeni, R. Moradian, S. Zinadini and B. Astinchap, *J. Membr. Sci.*, 2011, **375**, 284-294.
- 25 E. Celik, H. Park, H. Choi and H. Choi, *Water Res.*, 2011, **45**, 274-282.
- 26 H. A. Shawky, S. R. Chae, S. H. Lin and M. R. Wiesner, *Desalination*, 2011, **272**, 46-50.
- 27 M. Y. Lim, H. J. Kim, S. J. Baek, K. Y. Kim, S. S. Lee and J. C. Lee, *Carbon*, 2014, **77**, 366-378.
- 28 B. H. Yuan, C. L. Bao, L. Song, N. N. Hong, K. M. Liew and Y. Hu, *Chem. Eng. J.*, 2014, **237**, 411-420.
- 29 J. Q. Liu, C. F. Chen, C. C. He, L. Zhao, X. J. Yang and H. L. Wang, *ACS Nano*, 2012, **6**, 8194-8202.
- 30 Y. W. Cheng, S. T. Lu, H. B. Zhang, C. V. Varanasi and J. Liu, *Nano Lett.*, 2012, **12**, 4206-4211.
- 31 X. L. Yang, Y. Q. Zhan, J. Yang, J. C. Zhong, R. Zhao and X. B. Liu, *J. Polym. Res.*, 2012, **19**.
- 32 S. Y. Yang, W. N. Lin, Y. L. Huang, H. W. Tien, J. Y. Wang, C. C. M. Ma, S. M. Li and Y. S. Wang, *Carbon*, 2011, **49**, 793-803.
- 33 Y. Q. Li, T. Y. Yang, T. Yu, L. X. Zheng and K. Liao, *J. Mater. Chem.*, 2011, **21**, 10844-10851.
- 34 L. Qiu, X. W. Yang, X. L. Gou, W. R. Yang, Z. F. Ma, G. G. Wallace and D. Li, *Chem.-Eur. J.*, 2010, **16**, 10653-10658.
- 35 V. C. Tung, L. M. Chen, M. J. Allen, J. K. Wassei, K. Nelson, R. B. Kaner and Y. Yang, *Nano Lett.*, 2009, **9**, 1949-1955.

- 36 W. S. Hummers and R. E. Offeman, *J. Am. Chem. Soc.*, 1958, **80**, 1339-1339.
- 37 M. J. Yoo, H. W. Kim, B. M. Yoo and H. B. Park, *Carbon*, 2014, **75**, 149-160.
- 38 B. H. Jeong, E. M. V. Hoek, Y. S. Yan, A. Subramani, X. F. Huang, G. Hurwitz, A. K. Ghosh and A. Jawor, *J. Membr. Sci.*, 2007, **294**, 1-7.
- 39 K. P. Lee, T. C. Arnot and D. Mattia, *J. Membr. Sci.*, 2011, **370**, 1-22.
- 40 M. H. Liu, D. H. Wu, S. C. Yu and C. J. Gao, *J. Membr. Sci.*, 2009, **326**, 205-214.
- 41 S. Mallakpour and A. Zadehnazari, *Carbon*, 2013, **56**, 27-37.
- 42 B. Gebhardt, Z. Syrgiannis, C. Backes, R. Graupner, F. Hauke and A. Hirsch, *J. Am. Chem. Soc.*, 2011, **133**, 7985-7995.
- 43 S. Banerjee, T. Hemraj-Benny and S. S. Wong, *Adv. Mater.*, 2005, **17**, 17-29.
- 44 D. Silambarasan, K. Iyakutti and V. Vasu, *Chem. Phys. Lett.*, 2014, **604**, 83-88.
- 45 M. Hu and B. X. Mi, *Environ. Sci. Technol.*, 2013, **47**, 3715-3723.
- 46 D. Hanaor, M. Michelazzi, C. Leonelli and C. C. Sorrell, *J. Eur. Ceram. Soc.*, 2012, **32**, 235-244.
- 47 S. Qiu, L. G. Wu, L. Zhang, H. L. Chen and C. J. Gao, *J. Appl. Polym. Sci.*, 2009, **112**, 2066-2072.
- 48 A. Bassil, P. Puech, G. Landa, W. Bacsá, S. Barrau, P. Demont, C. Lacabanne, E. Perez, R. Bacsá, E. Flahaut, A. Peigney and C. Laurent, *J. Appl. Phys.*, 2005, **97**, 3.
- 49 S. Anantachaisilp, S. M. Smith, A. Treetong, S. Pratontep, S. Puttipatkhachorn and U. R. Ruktanonchai, *Nanotechnology*, 2010, **21**, 12-19.
- 50 C. Guiderdoni, E. Pavlenko, V. Turq, A. Weibel, P. Puech, C. Estourmes, A. Peigney, W. Bacsá and C. Laurent, *Carbon*, 2013, **58**, 185-197.
- 51 K. Ghosh, B. H. Jeong, X. F. Huang and E. M. V. Hoek, *J. Membr. Sci.*, 2008, **311**, 34-45.
- 52 S. Karan, S. Samitsu, X. S. Peng, K. Kurashima and I. Ichinose, *Science*, 2012, **335**, 444-447.
- 53 B. J. Hinds, N. Chopra, T. Rantell, R. Andrews, V. Gavalas and L. G. Bachas, *Science*, 2004, **303**, 62-65.
- 54 L. Q. Liu, A. H. Barber, S. Nuriel and H. D. Wagner, *Adv. Func. Mater.*, 2005, **15**, 975-980.
- 55 J. Glater, S. K. Hong and M. Elimelech, *Desalination*, 1994, **95**, 325-345.
- 56 P. Junwoo, C. Wansuk, S. H. Kim, B. H. Chun, B. Joona and K. B. Lee, *Desalin. Water Treat.*, 2010, **15**, 198-204.
- 57 H. M. Colquhoun, D. Chappell, A. L. Lewis, D. F. Lewis, G. T. Finlan and P. J. Williams, *J. Mater. Chem.*, 2010, **20**, 4629-4634.
- 58 X. M. Shi, B. B. Jiang, J. D. Wang and Y. R. Yang, *Carbon*, 2012, **50**, 1005-1013.
- 59 W. Zhou and L. Song, *Environ. Sci. Technol.*, 2005, **39**, 3382-3387.
- 60 American Society for Testing and Materials. Zeta potential of Colloids in Water and Waste Water. ASTM Standard D4187-82, **1985**.
- 61 E. M. V. Wagner, A. C. Sagle, M. M. Shar, and B. D. Freeman, *J. Membr. Sci.*, 2009, **345**, 97-109